Special Collection

Hybrid Sequences that Express both Aromatic Amide and α-Peptidic Folding Features

Xiaobo Hu,[b] Pradeep K. Mandal,[a] Brice Kauffmann,[c] and Ivan Huc*[a, b]

Foldamers combining aliphatic and aromatic main-chain units often produce atypical structures that cannot easily be accessed from purely aromatic or aliphatic sequences. We report solid-state evidence that sequences comprising α-amino acids and quinoline-based monomers adopt conformations that combine the folding propensities of both components. Foldamers **2** and **3** having an XQQ repeat motif (X = α-amino acid, Q = quinoline) were synthesized. Crystals of **2** (X = Phe, Q with an anionic side chain) obtained from water revealed an aromatic helix where amide groups belonging to the α-amino acids created a hydrogen-bond array typical of peptidic helices. Crystals of **3** (X = Ser, Q with a lipophilic side chain) obtained from organic solvents revealed a helix-turn-helix structure in which α-amino acid side chains interfere with main-chain hydrogen bonding. High sequence-dependency of the conformation is typical of peptides but is shown here to include aromatic folding features.

Introduction

Hybrid foldamers that combine building blocks with at least two distinct folding propensities have provided a rich ground for discovering new folding patterns.[1] Depending on the relative proportion of the building blocks, it has been shown that one type of building block may dominate the others and dictate its folding behavior. For example, the strong folding propensities of aromatic helices may template folding in flexible building blocks that would otherwise not adopt the same conformation or not fold at all.[2–4] Alternatively, the overall conformation may simultaneously reflect the folding behavior of both types of units and produce hybrid structures. In this respect, combining sp^3 centers and aromatic residues in the main chain has been particularly fruitful because a simple methylene group can promote a ~90° kink between aryl groups,[5,6] and completely change molecular shape. Herringbone helices,[7–9] spiral structures,[10] pillars[11,12] and knots[13,14] have been demonstrated in this way. Recently, structurally complex and unique foldamers were described using oligodisulfides of 1,3-phenylene-dithiols.[15] Occasionally, the folding propensities of the different units involved do not combine with one another in a consistent manner and long range order is lost.[16–18]

We have been interested in combining helical aromatic amide foldamers derived from 8-amino-2-quinoline carboxylic acid bearing side chains in position 4 (Q, Figure 1a) and α-amino acids because the latter are commercially available, and thus make it easy to increase side chain diversity, whereas each Q monomer to incorporate has to be synthesized prior to its use.[4,17,19]

Q_n sequences adopt a very stable helical conformation characterized by hydrogen bonds between amide NH protons and endocyclic quinoline nitrogen atoms, as well as by interactions associated with aromatic stacking (Figure 1b).[20,21] Aromatic amide helices thus have amide groups in planes perpendicular to the helix axis and tend to be side chain independent.[22] In contrast, peptide structures show extensive amide-amide hydrogen bonding. In 3_{10} or α-helices, amide groups belong to planes parallel to the helix axis. Furthermore, peptide structures are heavily influenced by the involvement of side chain functionalities. We previously showed that $LeuQ^{Leu}Q^{Leu}$-type sequence **1** (Figure 1c) can adopt aromatic helical conformations in chloroform, *i.e.* that folding is dominated by the quinoline groups.[4] Nevertheless, two sets of signals under slow exchange on the NMR time scale were observed, suggesting a bimodal folding behavior. A crystal structure of **1** allowed for the assignment of one of the species to a canonical aromatic helix with all amides in planes perpendicular to the helix axis (Figure 2a), while molecular modelling suggested that the other might involve direct hydrogen-bonding between amides belonging to the α-amino acids (Figure 2b). This means that **1** might combine aromatic amide folding with a hydrogen bonding pattern typical of α-peptides. In water, only one species was observed,[19] suggest-

[a] Dr. P. K. Mandal, Prof. I. Huc
Department Pharmazie and Center for Integrated Protein Science
Ludwig-Maximilians-Universität München
Butenandtstr. 5–13, 81377, München (Germany)
E-mail: ivan.huc@cup.lmu.de
[b] Dr. X. Hu, Prof. I. Huc
CBMN (UMR5248), Univ. Bordeaux-CNRS-IPB
Institut Européen de Chimie et Biologie
2 rue Robert Escarpit, 33600 Pessac (France)
[c] Dr. B. Kauffmann
IECB (UMS3033), Univ. Bordeaux-CNRS-INSERM
Institut Européen de Chimie et Biologie
2 rue Robert Escarpit, 33600 Pessac (France)

Supporting information for this article is available on the WWW under https://doi.org/10.1002/cplu.202000416

This article is part of a Special Collection on "Synthesis, Properties, and Applications of Foldamers"

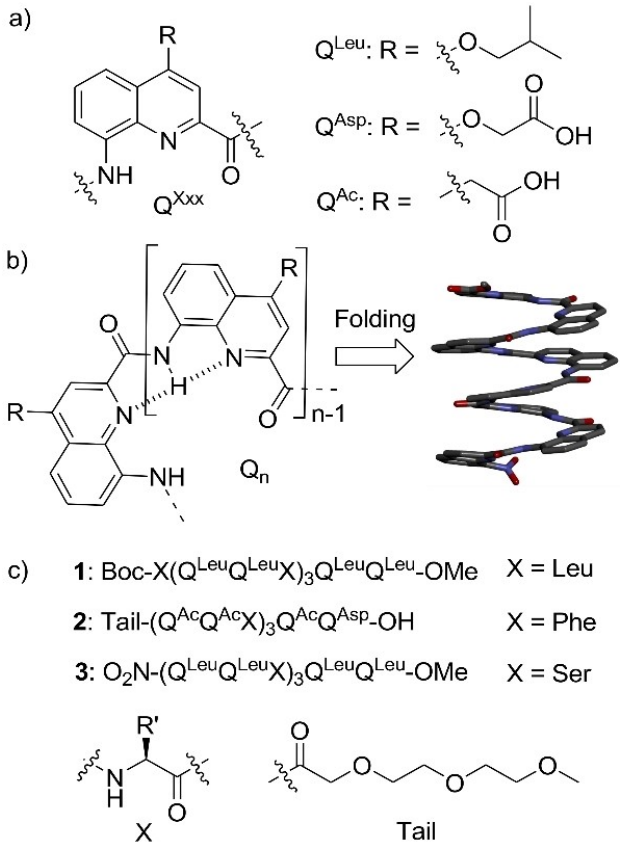

Figure 1. a) Structures of Q^{Xxx} residues. b) Principle of folding of a Q_n sequence. c) XQQ-type sequences **1**–**3**. In **3**, the *N*-terminal amine is replaced by an 8-nitro group.

ing tighter folding as can be expected from the contribution of hydrophobic effects.[21]

Here we present the synthesis and solid state structure of two new XQQ-type sequences (X = α-amino acid), one water soluble (**2**) and one organic soluble (**3**). The structures revealed two different combinations of aromatic foldamer and peptidic folding propensities. The water soluble sequence validated the co-existence of peptide-like amide hydrogen bonding within aromatic helices, as previously hypothesized based on modelling. It confirmed the robustness of $(XQQ)_n$ motifs to produce an array of α-amino acid side chains on one face of an aromatic helix. In contrast, sequence **3** showed that α-amino acid side chains can interfere with, and disrupt, canonical aromatic helices in organic solvents.

Results and Discussion

Design and synthesis

Sequences **2** and **3** were designed to combine good solubility in water (**2**) or organic solvents (**3**) and to possess features that favor crystal growth. The carboxymethyl-functionalized Q^{Ac} monomer used in sequence **2** has been previously shown to promote solubility in, and crystal-growth from, water.[22,23] A Q^{Asp} monomer was installed at the *C*-terminus because Q^{Ac} was known to undergo decarboxylation at this position.[22] The *N*-terminal diethylene glycol-derived tail of **2** also enhances water solubility. Conversely, the isobutoxy group of Q^{Leu} used in sequence **3** has been extensively shown to promote solubility in, and crystal growth ability from, chlorinated and aromatic solvents.[4,20] *N*-terminal nitro groups also tend to favor crystal growth. In addition, the two sequences were also endowed with features expected to promote aggregation. Exploiting the fact that an XQQ segment spans about one helix turn, the three α-amino acid residues of **2** and **3** were expected to be aligned on the same face of an aromatic helix (Figure 2a), and to promote aggregation, for example some sort of helix bundling. However, as shown in the following, no sign of the desired aggregation was found in the solid state. The three Phe residues were found to be insufficiently hydrophobic to lead to side chain-mediated aggregation or bundling of **2** in water. Similarly, **3** possesses Ser residues that may have promoted hydrogen-bond mediated aggregation in non-polar solvent if they were aligned. Eventually, the hydroxyl groups of the Ser residues were found to be involved in hydrogen bonds, but these were intramolecular, not intermolecular.

Sequences **2** and **3** were prepared using previously reported solid phase foldamer synthesis (SPFS) methods.[19,22] Crude **2** was obtained as a *C*-terminal carboxylic acid after cleavage from low-loading Wang resin with a trifluoroacetic acid (TFA)/triisopropylsilane/H_2O mixture. For **3**, cleavage was performed with a THF/methanol/1,8-diaza-bicyclo[5.4.0]undec-7-ene mixture to directly yield a *C*-terminal methyl ester. An additional reaction step with TFA was then required to deprotect the hydroxyl groups on Ser residues. Pure product **2** was obtained after semi-preparative RP-HPLC separation. Compound **3** proved to be too lipophilic for RP-HPLC and was purified by preparative thin layer chromatography (see Experimental Section).

Structure of 2

Crystals of **2** were obtained using standard sitting and hanging drop vapor diffusion methods and screening conditions suited for for poly-anions. As expected, the short side chains of Q^{Ac} were effective at promoting crystal growth. Single crystals grew without having to resort to racemic crystallography as it had been the case for **1**[4] and other aromatic amide foldamers bearing chiral groups.[8,24] The synthesis of the (D)-enantiomer of **2** was thus not necessary. The structure of **2** was solved at atomic resolution in the $P2_12_12_1$ space group (Figure 2c, d). The asymmetric unit contains two molecules having very similar conformations, including with regards to side chain orientation. The structure is that of a *P*-helix, as previously observed when using (L)-α-amino acids. It superimposes with the model initially proposed for **1** (Figure 2b) which is remarkable considering that the structural model of **1** was produced by a short molecular dynamics simulation in $CHCl_3$ as a non-explicit solvent, and with no experimental input.[4] Thus, the structure of **2** consists of an aromatic helix in which every third amide group, that is, every

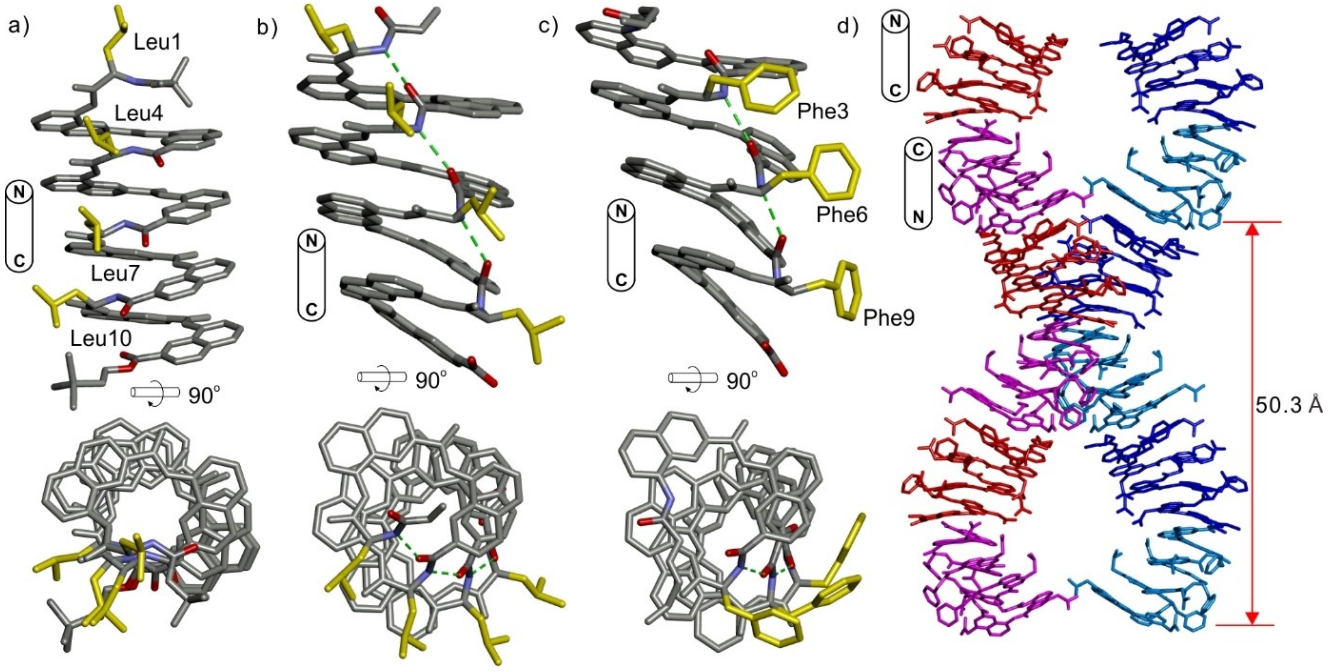

Figure 2. a) Crystal structure of **1**. b) Energy-minimized model of an alternate conformation of **1**.[4] c) Crystal structure and d) crystal packing of **2**. Small cartoons indicate the helices' *C*- and *N*-termini. In a)–c), quinoline side chains, hydrogen atoms and some terminal functions are omitted for clarity; α-amino acid side chains are highlighted in golden; investigated amide bonds have their O and N atoms shown in red and blue, respectively; some key hydrogen bonds are shown as dashed green lines. In d) helices are shown in different colours for clarity: red and magenta in one helix stack, and blue and azure in the other.

amide NH-CO preceding a Phe residue, is not coplanar to the neighboring quinoline ring. Instead, a tilt of about 50° is observed. These tilted amide groups form an array of hydrogen bonds that are nearly parallel to the helix axis as in a regular peptide α-helices. Thus, this builds up a macrodipole. However, because the tilted amide carbonyl groups point towards the *N*-terminus, the macrodipole has an opposite orientation to that of an α-helix. The tilt is made possible by a rotation about some aryl-carbonyl bonds which locally disrupts conjugation and 2-quinolinecarboxamide five-membered hydrogen-bonded rings. Indeed, rotation about the aryl-carbonyl bond has been calculated[25] and observed[26] to have the lowest barrier in quinoline carboxamide foldamers, as opposed to rotation about the aryl-NH or the amide bonds. As a result of the array of hydrogen bonds involving aliphatic amides, helical curvature is somewhat decreased with respect to that of the helix of **1** observed in the solid state (Figure 2a). Consequently, instead of a linear array, the three Phe side chains form a helical array (Figure 2c, bottom) where each PheQQ segment spans a little less than a turn.

The structure of **2** thus stands as an original example of a conformation that combines the folding features of two distinct, and a priori incompatible, building blocks. The combination nevertheless brings some frustrations such as the rotated aryl-carbonyl groups mentioned above, as well as the exact α-amino acid conformations. Indeed, examining ϕ and ψ values of the Phe residues (Table 1) and plotting them in a Ramachandran plot (Figure 3, red triangles) highlighted that they were out of the favored area of peptide α-helix and β-sheet conformations.

Table 1. Summary of ϕ and ψ dihedral angles of α-amino acid residues of foldamers **1**–**3**.

Foldamer **1**	Leu4[a]	Leu7[a]	Leu10[a]
ϕ	−143°	−140°	−155°
ψ	26°	40°	35°
Foldamer **2**	Phe3[b]	Phe6[b]	Phe9[b]
ϕ	64.3°	72.3°	65.5°
ψ	24.0°	17.2°	23.9°
Foldamer **3**	Ser3[b]	Ser6[b]	Ser9[b]
ϕ	−139.1°	−161.4°	−146.3°
ψ	18.1°	−170.7°	4.7°

[a] From previously reported data.[4] [b] Numbers indicate the position in the sequence counted from the *N*-terminus. For each sequence, there are two sets of dihedral angle value (see Table S2) and the averaged ϕ and ψ values are shown here.

Instead, they are located near the rare left-handed α-helix area. This is indeed consistent with their belonging to a right-handed helix but with a macrodipole opposite to that of right-handed α-helices, i.e. with amide groups in an opposite direction. In comparison, the crystal structure of the LeuQ^{Leu}Q^{Leu}-type foldamer **1** had ψ and ϕ values near those of β-strands. The interconversion between the structure of **1** and that of **2** thus requires little change of ψ but a major change of ϕ (Table 1, Figure 2a and 3).[4]

The Phe side chains were found to be folded back on the helix (Figure 2c). They presumably constitute a hydrophobic patch at the helix surface but this was not expressed in the crystal packing. Helix-helix contacts were not guided by intermolecular proximity between Phe residues. The NMR

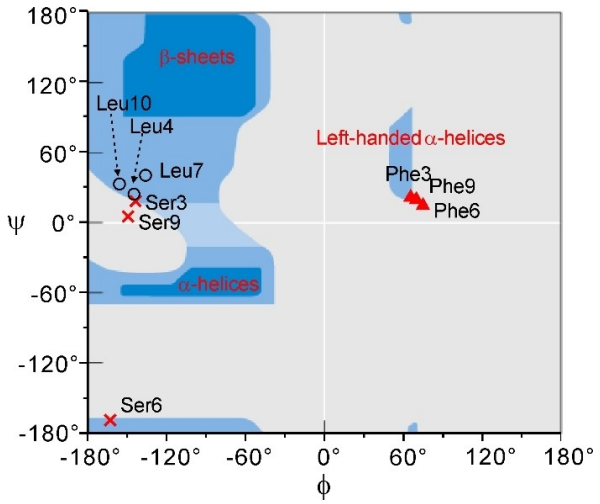

Figure 3. The coordinates of the ϕ and ψ dihedral angles of Table 1 shown on a Ramachandran plot. Dark blue and light blue indicate the very common, and common, respectively, α-amino acid conformations in peptides and proteins. Phe3,6,9, Ser3,6,9 and Leu4,7,10 are shown as red triangles, red crosses and black circles, respectively.

spectrum shows one species and slightly broadened signals, suggesting that, if aggregation occurs, the different states are short lived and equilibrate rapidly (see the Supporting Information). In the absence of a strong indication of aggregation, this was not investigated further. Nevertheless, the NMR spectrum shows only one set of signals as was previously observed for another water soluble variant,[19,27] indicating that the slow equilibrium between two folded states observed for **1** (Figure 2a, 2b) occurs only in organic solvents and that the structure is better defined in water. The CD spectrum of **2** (Figure S3) shows a positive band at 370 nm confirming the right-handed helicity observed in the solid state structure and in agreement with the CD spectrum of **1**.[4]

The crystal packing nevertheless revealed original features. Helices were found to stack head-to-head and tail-to-tail via their aromatic cross-sections to form a continuous one-handed supramolecular helix. However, unlike the stacks of Q_n sequences previously reported,[22,23,28] and contrary to the crystal structure of **1**, the supramolecular helix was not cylindrical but undulating (Figure 2d, Figure S1). The undulation was apparently caused by the *N*-terminal and *C*-terminal helix cross-sections not being in parallel to each other, and by the *C*-terminal cross-section being tilted with respect to the helix axis. Stacking at the *C*-terminus thus creates a bend in the stack which is reversed by a 2_1 screw axis. The pitch of the 2_1 axis is 50.3 Å (long axis of the unit cell). The undulation generates a distinct shape that seems to guide packing in parallel planes, each plane consisting of interdigitated undulating helices (Figure S1b). Within these planes, the different undulating helices are also connected by bridging calcium ions between carboxylate residues, as was previously encountered in the structure of other anionic foldamers[22,23] and as frequently seen in the crystal structures of nucleic acids. When looking at undulating helices belonging to neighboring planes, undulation was found to be offset, thus leading to a peculiar shape resembling that of an X chromosome (Figure 2d).

Structure of 3

Crystals of **3** were obtained by slowly diffusing CH_3CN into a dichloromethane solution. As for **2**, racemic crystallization was not required to obtain X-ray quality single crystals and the structure was solved at atomic resolution. Again two almost superimposable molecules constitute the asymmetric unit. They revealed a completely different pattern yet again expressing both aromatic amide and α-peptidic folding features (Figure 4). Instead of a consistent helix, a helix-turn-helix-like structure (HTH) was found with two right-handed aromatic helical segments separated by an extended turn. The conformation appeared to be driven by hydrogen bonds involving the serine hydroxyl group,[29] reflecting a prominent feature of α-peptides, and in contrast with the side chain-independent nature of Q_n aromatic helices. Starting from the *N*-terminus, the first five residues generate a *P* helix as previously observed in the structure of **1** (Figure 2a). The hydroxyl group of Ser3 forms a

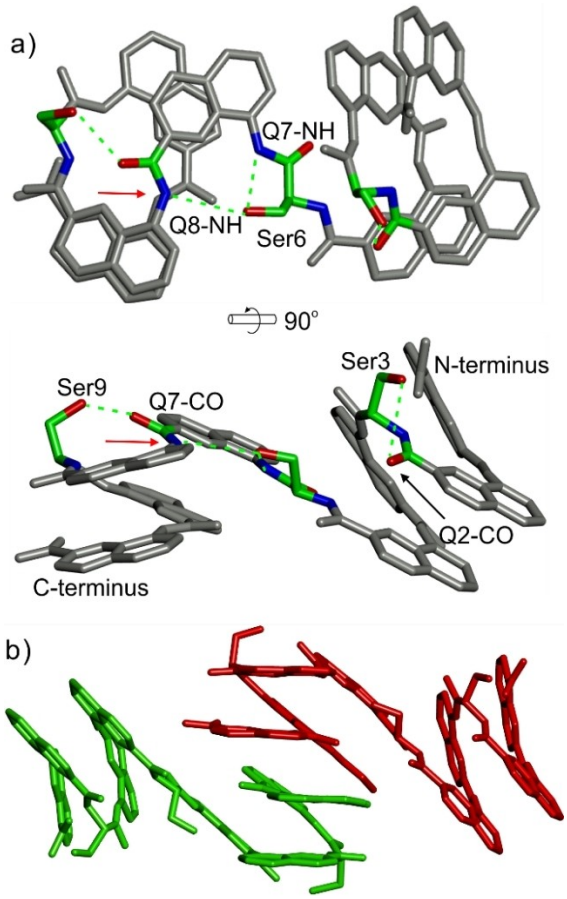

Figure 4. Crystal structure of **3**. Quinoline side chains, H atoms and some terminal functions are omitted for clarity. In a), Ser residues and some key amide functions are highlighted with their C, O and N atoms in green, red and blue, respectively. Hydrogen bonds are shown as dashed green lines. The twisted aryl-NH bond Q8-NH is indicated by red arrows. In b), molecules are colored in green or red to show the head-to-head stacking.

seven-membered hydrogen-bonded ring with the contiguous Q2-CO ($d_{O-O}=3.4$ Å) compatible with the aromatic helix motif. Ser6 is found in the turn where folding deviates from previously observed structures. Its hydroxy oxygen atom is hydrogen-bonded by two NH groups (Q7-NH $d_{N-O}=2.9$ Å; Q8-NH$d_{N-O}=$ 3.4 Å). As a consequence, Q7 does not stack on the first helical segment and initiate a new helix. The availability of Q8-NH for hydrogen bonding results from a twist to aromatic folding rules in the structure. The Q8-NH bond is indeed rotated by 140°, in contrast with other Q-NH bonds which are all below 18°. This rotation entails a local disruption of conjugation and of a five-membered hydrogen-bonded ring. It is facilitated by the involvement of the hydroxy group of Ser9 which hydrogen bonds to the Q7-CO ($d_{O-O}=3.0$ Å).

The ϕ and ψ dihedral angles of the Ser residues were measured and included in a Ramachandran plot (Table 1, Figure 3, red crosses). Consistent with their roles in the helical segments of **3**, Ser3 and Ser9 have ϕ and ψ values close to those found in **1**, *i.e.* close to those typical of β-sheets. Values for Ser6 were also close to those of β-sheets but at the other end of the range ($\psi=-171°$). The contrasting behavior of **1** and **3** that follows the replacement of Leu by Ser is typical of peptides in which a single mutation may result in a conformational change, *e.g.* from a β-strand to an α-helix.[30] Whether the solid state conformation **3** also prevails in solution was not investigated. The NMR spectrum in $CDCl_3$ is somewhat broad (see the Supporting Information) indicating dynamics associated with possible conformational changes and aggregation. Since **1** itself exists as a mixture of conformers in slow exchange on the NMR time scale, the broad NMR spectrum of **1** was not suggestive of a well-organized structure. Nevertheless, the CD spectrum of **3** (Figure S4) also shows a positive band at 370 nm in agreement with the right-handed helicity observed in the solid state. One may speculate that the solid state structure of **3** would not be favored in water (pending a water soluble analogue is produced) since it entails the disruption of some aromatic stacking which is enhanced by hydrophobic effects.

With respect to crystal packing, the HTH offers more aromatic surface, furthermore in varied orientations, than a single helix, leading to multiple possibilities for stacking. The outcome was found to be rather complicated. Besides the *C*-terminal head-to-head stacking shown in Figure 4b, contacts between the *N*-terminal cross section and a quinoline adjacent to the turn was observed (Figure S2a). Each molecule was thus found to be stacked to three others. Stacking involving the *N*-terminal cross-section resulted in layers of zig-zag tapes (Figure S2b) while stacking involving the *C*-terminal cross-section connected the layers. No noticeable intermolecular hydrogen bonding was noted.

Conclusion

In summary, we now have three crystal structures of XQQ-type sequences that all have demonstrated different folding modes, involving the main chain amide and the side chain of the α-amino acids to various degrees. The structures obtained from organic solvents suggest only moderate, sequence dependent, conformation control in this medium. The flexibility introduced by α-amino acids provides significant conformational freedom and side chains may then interfere with main chain folding preferences, leading to original structures such as that of **3**. In contrast, the structure crystallized from water indicates fulfillment of hydrophobic effects in an aromatic helix in a manner compatible with main chain hydrogen bonding typical of α-peptide structures. This leads to the formation of a macrodipole not observed before in aromatic helices. This conformation is presumed to be more robust and not sequence dependent, which offers possibilities for decorating helices with defined arrays of side chains at their surface. In retrospect, and after having observed the structure of **3**, it may be noted that the hydrophobic Phe side chains in **2** do not alter aromatic stacking within the helix in water. The structure of **2** also corroborates the efficacy of short polar side chains at facilitating crystal growth.[22] The initial objective of promoting well defined helix aggregation was, however not reached. Future efforts in this direction include increasing hydrophobicity at the helix surface and introducing side chains that may promote salt bridges as seen in α-peptide helix bundles.

Experimental Section

General Procedures: All reagents, unless otherwise specified, were purchased from commercial sources, and used without further purification. Anhydrous tetrahydrofuran (THF) and dichloromethane (DCM) were dispensed from a solvent purification system. *N*,*N*-Diisopropylethylamine (DIPEA) was distilled over CaH_2 prior to use. Milli-Q water and HPLC grade acetonitrile were used for RP-HPLC analyses and purification. Fmoc-$Q^{Asp(tBu)}$-OH, Fmoc-Q^{Leu-}OH and Fmoc-$Q^{Ac(tBu)}$-OH were prepared as previously reported.[22,31] Procedures for *i*) Wang resin bromination; *ii*) resin loading; *iii)* Fmoc protecting group removal; *iv*) acid chloride activation and coupling (for quinoline monomers and the tail); *v*) *in situ* acid chloride coupling of *N*-Fmoc-(*L*)-α-amino acids; *vi*) on resin *C*-terminal transesterification (for sequence **3**); *vii*) side chain deprotection and resin cleavage were followed as previously reported as well.[19,22,31] SPFS was carried out manually using a CEM Discover microwave oven at atmospheric pressure and a vacuum-filtration station using an open-vessel mode. The resin and reaction mixture were placed in the reactor vessel and the temperature of reaction was monitored by a fiber optic temperature probe. ^{1}H NMR spectra were recorded at 300 MHz. Chemical shifts were reported in ppm and were calibrated against residual solvent signals of DMSO-d_6 ($\delta=2.50$ ppm), or to the reference signal of TMS ($\delta=0.00$ ppm) (10 μM 3-(trimethylsilyl)-1-propanesulfonic acid sodium salt in H_2O/D_2O (9:1, vol/vol)). Coupling constants were reported in Hz and signal multiplicities were abbreviated as s, singlet; d, doublet; m, multiplet or overlapped signals; and br, broad. Silica gel chromatography was performed by using Merck TLC Silica gel 60 F_{254} (aluminium sheets 20×20 cm). RP-HPLC analyses were carried out at 1.0 mL min^{-1} by using a Macherey-Nagel Nucleodur C18 gravity column (4.6×100 mm, 3 μm). The mobile phase was composed of 12.5 mM NH_4Ac-NH_4OH in MilliQ-H_2O (pH = 8.5, solvent A) and acetonitrile (solvent B). Elution was monitored by UV detection at 214, 254 and 300 nm with a diode array detector. Purification of crude oligoamide **2** from SPS was carried out by semi-preparative RP-HPLC at a 3.0 mL min^{-1} flow using a Macherey-Nagel Nucleodur C18 HTEC column (21 mm×125 mm, 5 μm). The solvents of semi-

preparative RP-HPLC were the same as analytical RP-HPLC. Monitoring was performed by UV detection at 254 and 300 nm with a diode array detector. High-resolution electrospray ionization time of flight (ESI-TOF) mass spectra were obtained in positive ion mode.

Synthetic Method: Compound **2** was synthesized on a 10.25 μmol scale (25 mg of Wang resin, manufacturer's loading 0.41 mmol.g^{-1}). The crude product was purified by semi-preparative RP-HPLC (15-25% B, over 15 min) to afford the expected compound as a white solid (6.5 mg, 26%, purity by RP-HPLC: 97%). RP-HPLC (15-25% B, over 7 min) $R_t = 6.7$ min. ^{1}H NMR (300 MHz, 10% D_2O/H_2O vol/vol): $\delta = 11.45–11.20$ (br, 4H), 8.90–8.68 (br, 4H), 8.68–8.40 (br, 4H), 8.29–6.80 (m, overlapping with NH_4^+ ions signal), 4.25–4.01 (m, 6H), 3.45–2.65 (m, 29H). HRMS: calcd. for $C_{130}H_{106}N_{19}O_{33}$ $[M+H]^+$ 2460.7200; found 2460.7225.

Compound **3** was synthesized on a 10.25 μmol scale (25 mg of Wang resin, manufacturer's loading 0.41 mmolg^{-1}). Through on resin transesterification with MeOH, the product was cleaved from resin as a methyl ester bearing side chain protection (**3**-pro). After evaporating organic solvents, crude **3**-pro was allowed to precipitate in 5% citric acid aqueous solution and it was further purified by silica gel column chromatography (100% DCM). Afterwards, side chain deprotection was carried out in a TFA/DCM solution (50:50 vol/vol) at room temperature for 4 hours to afford crude compound **3**. Due to its high hydrophobicity and the limited amount of material, purification was performed by thin layer chromatography (aluminium sheets, 20×20 cm). After collecting the silica gel layer only containing the desired product, expected compound 3 was washed out with DCM, concentrated and precipitated in Et_2O to yield a yellow solid (3.6 mg, 15%). ^{1}H NMR (300 MHz, DMSO-d_6): $\delta =$ 11.19 (s, 1H), 10.99 (br, 2H), 10.54 (br, 2H), 10.34 (s, 1H), 10.05 (s, 1H), 8.91–8.77 (m, 3H), 8.55–8.45 (m, 1H), 8.18 (d, $J = 9.0$ Hz, 1H), 7.98 (br, 1H), 7.74–7.52 (m, 10H), 7.46 (s, 1H), 7.43–7.12 (m, 9H), 7.10–6.92 (m, 4H), 6.87–6.71 (m, 3H), 6.62 (br, 1H), 6.39 (s, 1H), 5.20–4.99 (m, 2H), 4.80 (br, 1H), 4.40 (br, 1H), 4.22–3.68 (m, 18H), 3.65–3.35 (m, overlapped with water peak), 2.37–2.27 (m, 2H), 2.22–2.10 (m, 6H), 1.29–1.03 (m) ppm. HRMS: calcd. for $C_{122}H_{130}N_{19}O_{25}$ $[M+H]^+$ 2260.9485; found 2260.9613.

Methods for X-ray crystallography (see the Supporting Information for details): A 2.5 mM stock solution of **2** in 12.5 mM ammonium acetate was prepared for crystallization screening trials with sparse matrix commercial screens using the sitting drop vapour diffusion method at 293 K. X-ray quality crystals were optimized using the hanging drop method by adding 0.5 μL of **2** and 1.5 μL of reservoir solution: 30% w/v PEG 4000, 50 mM TRIS buffer (pH 8.5), 150 mM ammonium chloride and 10 mM calcium chloride. Single crystals were fished using microloops, flash cooled in liquid nitrogen and sent for low temperature X-ray diffraction at the ID30b beamline in ESRF, Grenoble.[32] The crystal diffracted to atomic resolution and a data set was measured using a Pilatus 6 M detector. X-ray quality crystals of compound **3** were grown by slowly diffusing CH_3CN into a dichloromethane solution. Single crystals were quickly soaked in Paratone-N oil and flash frozen. Diffraction data were collected at the IECB X-ray facility using a 3 kW microfocusRigaku FRX rotating anode (Cu Kα wavelength) and a hybrid Dectris Pilatus 200 K detector.

Diffraction data for **2** and **3** were processed using *XDS*[33] and *CrystalClear*.[34] Both structures were solved with *ShelxD*[35] and refined by full-matrix least square method on F^2 with ShelxL-2014[36] within Olex2.[37] For all atoms Anisotropic atomic parameters were used. Hydrogen atoms were placed at idealized positions and refined as riding of their carriers with Uiso(H) = 1.2Ueq(CH, CH2, NH) and Uiso(H) = 1.5Ueq(CH3). DFIX, AFIX, FLAT, EADP and DELU instructions were used to improve the geometry and thermal parameters. Severely disordered solvent molecules were removed using the SQUEEZE procedure from PLATON suite.[38] Crystallographic data, refinement statistics and comments on checkcif alerts obtained from IUCr's checkcif algorithm are reported in supporting information. https://www.ccdc.cam.ac.uk/services/structures?id=doi:10.1002/cplu.202000416 Deposition Numbers 955282 (for **1**), 2002649 (for **2**), and 2002410 (for **3**) contain the supplementary crystallographic data for this paper. These data are provided free of charge by the joint Cambridge Crystallographic Data Centre and Fachinformationszentrum Karlsruhe Access Structures service https://www.ccdc.cam.ac.uk/structures.

Acknowledgements

The authors would like to thank China Scholarship Council for a PhD scholarship for X. Hu. This work was supported by the European Research Council under the European Union's Seventh Framework Programme (Grant Agreement No. ERC-2012-AdG-320892). It benefited from the facilities and expertise of the Biophysical and Structural Chemistry platform at IECB, CNRS UMS3033, INSERM US001, Université de Bordeaux. We thank Dr. L. Fischer for assistance with CD measurements. Open access funding enabled and organized by Projekt DEAL.

Conflict of Interest

The authors declare no conflict of interest.

Keywords: foldamers · helices · hybrid sequences · hydrogen bonding · peptides

[1] A. Roy, P. Prabhakaran, P. K. Baruah, G. J. Sanjayan, *Chem. Commun.* **2011**, *47*, 11593–11611.
[2] C. Dolain, J.-M. Léger, N. Delsuc, H. Gornitzka, I. Huc, *Proc. Natl. Acad. Sci. USA* **2005**, *102*, 16146–16151.
[3] D. Sánchez-García, B. Kauffmann, T. Kawanami, H. Ihara, M. Takafuji, M.-H. Delville, I. Huc, *J. Am. Chem. Soc.* **2009**, *131*, 8642–8648.
[4] M. Kudo, V. Maurizot, B. Kauffmann, A. Tanatani, I. Huc, *J. Am. Chem. Soc.* **2013**, *135*, 9628–9631.
[5] N. G. Angelo, P. S. Arora, *J. Am. Chem. Soc.* **2005**, *127*, 17134–17135.
[6] N. Raynal, M.-C. Averlant-Petit, G. Bergé, C. Didierjean, M. Marraud, C. Duru, J. Martinez, M. Amblard, *Tetrahedron Lett.* **2007**, *48*,1787–1790.
[7] N. Delsuc, F. Godde, B. Kauffmann, J.-M. Léger, I. Huc, *J. Am. Chem. Soc.* **2007**, *129*,11348–11349.
[8] M. Kudo, D. C. López, V. Maurizot, H. Masu, A. Tanatani, I. Huc, *Eur. J. Org. Chem.* **2016**, 2457–2466.
[9] M. Akazome, Y. Ishii, T. Nireki, K. Ogura, *Tetrahedron Lett.* **2008**, *49*, 4430–4433.
[10] C. A. Hunter, A. Spitaleri, S. Tomas, *Chem. Commun.* **2005**, 3691–3693.
[11] R. S. Lokey, B. L. Iverson, *Nature*, **1995**, *375*, 303–305.
[12] S. Ghosh, S. Ramakrishnan, *Angew. Chem. Int. Ed.* **2004**, *43*, 3264–3268; *Angew. Chem.* **2004**, *116*, 3326–3330.
[13] J. Brüggemann, S. Bitter, S. Müller, W. M. Müller, U. Müller, N. M. Maier, W. Lindner, F. Vögtle, *Angew. Chem. Int. Ed.* **2006**, *46*, 254–259.
[14] N. Ponnuswamy, F. B. L. Cougnon, J. M. Clough, G. D. Pantoş, J. K. M. Sanders, *Science*, **2012**, *338*, 783–785.
[15] B. Liu, C. G. Pappas, E. Zangrando, N. Demitri, P. J. Chmielewski, S. Otto, *J. Am. Chem. Soc.* **2019**, *141*,1685–1689.
[16] D. Srinivas, R. Gonnade, S. Ravindranathan, G. J. Sanjayan, *J. Org. Chem.* **2007**, *72*, 7022–7025.
[17] M. Kudo, V. Maurizot, H. Masu, A. Tanatani, I. Huc, *Chem. Commun.* **2014**, *50*, 10090–10093.

[18] L. Milli, M. Larocca, M. Tedesco, N. Castellucci, E. Ghibaudi, A. Cornia, M. Calvaresi, F. Zerbetto, C. Tomasini, *J. Org. Chem.* **2014**, *79*, 5958–5969.
[19] X. Hu, S. J. Dawson, Y. Nagaoka, A. Tanatani, I. Huc, *J. Org. Chem.* **2016**, *81*, 1137–1150.
[20] H. Jiang, J.-M. Léger, I. Huc, *J. Am. Chem. Soc.* **2003**, *125*, 3448–3449.
[21] T. Qi, V. Maurizot, H. Noguchi, T. Charoenraks, B. Kauffmann, M. Takafuji, H. Ihara, I. Huc, *Chem. Commun.* **2012**, *48*, 6337–6339.
[22] X. Hu, S. J. Dawson, P. K. Mandal, X. de Hatten, B. Baptiste, I. Huc, *Chem. Sci.* **2017**, *8*, 3741–3749.
[23] V. Corvaglia, D. Carbajo, P. Prabhakaran, K. Ziach, P. K. Mandal, V. Dos Santos, C. Legeay, R. Vogel, V. Parissi, P. Pourquier, I. Huc, *Nucleic Acids Res.* **2019**, *47*, 5511–5521.
[24] C. Dolain, H. Jiang, J.-M. Léger, P. Guionneau, I. Huc, *J. Am. Chem. Soc.* **2005**, *127*, 12943–12951.
[25] A. M. Abramyan, Z. Liu, V. Pophristic, *Chem. Commun.* **2016**, *52*, 669–672.
[26] K. Urushibara, Y. Ferrand, Z. Liu, H. Masu, V. Pophristic, A. Tanatani, I. Huc, *Angew. Chem. Int. Ed.* **2018**, *57*, 7888–7892; *Angew. Chem.* **2018**, *130*, 8014–8018.
[27] Reference [19] also reports an NMR structure elucidation in aqueous solution of an XQQ type foldamer. However, we think there are issues with the final proposed structure due to the fact that incorrect charges were used during the energy minimization step. This NMR structure was not reinvestigated but we believe it is likely to match the crystal structure of **2** reported here.
[28] S. R. Post, B. Langlois d'Estaintot, T. Granier, C. D. Mackereth, L. Fischer, I. Huc, *Chem. Eur. J.* **2019**, *25*, 11042–11047.
[29] The hydroxy protons were not visible in the electron density map and their positions could only be inferred from those of neighboring hydrogen bond acceptors.
[30] W.-Z. Yang, T.-P. Ko, L. Corselli, R. C. Johnson, H. S. Yuan, *Protein Sci.* **1998**, *7*, 1875–1883.
[31] B. Baptiste, C. Douat-Casassus, K. Laxmi-Reddy, F. Godde, I. Huc, *J. Org. Chem.* **2010**, *75*, 7175–7185.
[32] C. Mueller-Dieckmann, M. W. Bowler, P. Carpentier, D. Flot, A. A. McCarthy, M. H. Nanao, D. Nurizzo, P. Pernot, A. Popov, A. Round, A. Royant, D. de Sanctis, D. von Stetten, G. A. Leonard, *Eur. Phys. J. Plus* **2015**, *130*, 70.
[33] W. Kabsch, *Acta Crystallogr.* **2010**, *D66*, 125–132.
[34] Crystal Clear and Crystal Structure, Rigaku/MSC, The Woodlands, TX, 2005.
[35] G. M. Sheldrick, *Acta Crystallogr.* **2008**, *A64*, 112–122.
[36] G. M. Sheldrick, *Acta Crystallogr.* **2015**, *C71*, 3–8.
[37] O. V. Dolomanov, L. J. Bourhis, R. J. Gildea, J. A. K. Howard, H. Puschmann, *J. Appl. Crystallogr.* **2009**, *42*, 339–341.
[38] A. L. Spek, *Acta Crystallogr.* **2009**, *D65*, 148–155.

Manuscript received: May 27, 2020
Revised manuscript received: July 5, 2020
Accepted manuscript online: July 6, 2020